Cambridge University Press
978-0-521-76995-2 - Theory of Molecular Rydberg States
M. S. Child
Excerpt
More information

1

Molecular Rydberg states

1.1 The nature of Rydberg states

The nature of atomic Rydberg states is well described by Gallagher, though with less emphasis on theory [1]. Those of molecules are severely complicated by the additional nuclear degrees of freedom, in a way that gives them quite different properties from those treated in most spectroscopic texts [2, 3, 4, 5]. The essential difference is that established spectroscopic theory is rooted in the Born–Oppenheimer approximation, whereby the frequencies of the electronic motion are assumed to be so high compared with the vibrational and rotational ones that the nuclear motions may be treated as moving under an adiabatic electronic energy (or potential energy) surface. In addition the vibrational frequency usually far exceeds that of the rotations, which means that every vibrational state has an approximate rotational constant. Such considerations provide the basis for a highly successful systematic theory. Modern *ab-initio* methods allow the calculation of very reliable potential energy surfaces and there are a variety of efficient methods for diagonalizing the resulting Hamiltonian matrix within a functional or numerical basis. Electronically non-adiabatic interactions between a small number of electronic states can also be handled by this matrix diagonalization approach, even including fragmentation processes, if complex absorbing potentials are added to the molecular Hamiltonian.

The difficulty in applying such techniques to highly excited molecular electronic states is that the Rydberg spectrum of every molecule includes 100 electronic states with principal quantum number $n = 10$, separated from the $n = 11$ manifold by only 100 cm^{-1}, which is small compared with most vibrational spacings and comparable to rotational spacings for small hydride species. Figure 1.1 shows a simplified level scheme for a species with a positive ion rotational constant, $B = 30\ \mathrm{cm}^{-1}$, and a vibrational interval, $\omega = 2322\ \mathrm{cm}^{-1}$, appropriate to H_2^+. The levels

CAMBRIDGE

Cambridge University Press
978-0-521-76995-2 - Theory of Molecular Rydberg States
M. S. Child
Excerpt
More information

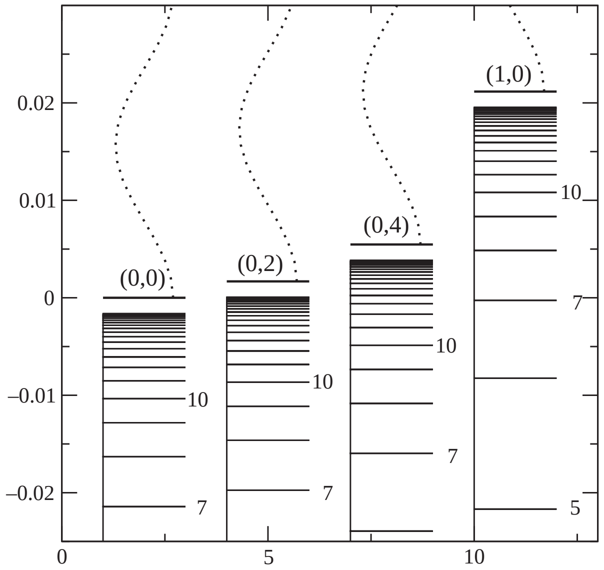

Figure 1.1 A schematic molecular Rydberg system, showing series terminating on different (v, J) energy levels of the positive ion. The isolated solid lines mark the series limits. The wavy dotted lines are the attached continua. Small labels are the principal quantum numbers, n. Energies are measured in atomic units from the (0, 0) ionization limit.

are calculated by the Rydberg formula

$$E_{nv^+J^+} = E^+_{v^+N^+} - \frac{R_y}{(n-\mu)^2}, \tag{1.1}$$

with the quantum defect $\mu = 0.169$ appropriate to the np $^1\Sigma_u^+$ system of H_2. Each series, whose continuum is marked by a wavy dotted line, is labelled by the vibrational rotational quantum numbers (v^+, N^+). The small symbols, marking individual levels are the principal quantum numbers, n. One sees for example that the $n = 10$ level of the $(0, 2)$ series lies above the $n = 11$ level of the $(0, 0)$ series, which means that the electronic energy splitting is smaller than the $\Delta N^+ = 0 \rightarrow 2$ rotational interval. In addition, the perturbations arising from the resulting non-adiabatic coupling in the discrete spectrum go over to auto-ionization as soon as discrete members of a higher series lie in the continuum of a lower one. The situation with regard to the $^1\Sigma_g^+$ series of H_2 is further complicated by interaction with ion-pair valence states, which give rise to the famous double minimum pairs (E,F), (G,H), etc.

It is therefore evident that Rydberg systems require a theory that can handle the presence of bound and slowly fragmenting states in a unified way. The method of choice is ‘multichannel quantum defect theory’ or MQDT, which visualizes the dynamics as a scattering process in which collisions between the loosely bound electron and a short-range positive ion core lead to phase changes and energy transfer probabilities that determine the physical observables [6, 7, 8, 9]. An important difference from normal scattering theory is that the electron is scattered into an attractive Coulomb field, rather than a field-free region. Thus for example a low-lying bound electron may be scattered to and fro between neighbouring bound states, leading to spectral perturbations. Another possibility is that the collisions may excite the positive ion into a dissociative electronic state, leading to molecular predissociation. The dynamics are further complicated for higher-lying bound states by the possibility of scattering into the ionization continuum.

Fortunately there is a major simplification, in that the energy range of most interest in molecular physics is small compared with the total energy of the system. Consequently the parameters, loosely termed 'quantum defects', that characterize the fundamental collision process, may often be treated as almost independent of energy over the physically interesting range. The dynamical complications arise principally from the boundary conditions of the coupled system.

The quantum defects may be treated at one level as phenomenological parameters, to rationalize the observations. As a simple example, the Rydberg formula for the energies of alkali atoms

$$E_{n\ell} = I - \frac{R_y}{(n - \mu_\ell)^2}, \tag{1.2}$$

with $\mu_2 > \mu_{\mathrm{p}} > \mu_{\mathrm{d}}$, etc., is well known to allow fairly accurate predictions of entire series, from observation of a single member – even without allowing for the weak energy dependence of the quantum defect parameters, μ_ℓ. Similarly, as a slightly more complicated example, analysis of the perturbations between bound levels below the first ionization limit in Fig. 1.1 may be used to predict the rates of autoionization above the limit. Another benefit of the weak energy dependence concerns the relevance of *ab-initio* electronic structure theory. Standard techniques [10] can now yield highly accurate low-lying potential energy functions for small molecules, including Rydberg states up to $n \simeq 4$, but the extension to higher members of the series is prohibitive because the very diffuse outer parts of the orbitals are poorly approximated by Gaussian functions. By contrast, MQDT techniques work with exact Coulomb wavefunctions in the outer region, and the necessary interactions with the core may be extracted as quantum defect functions, from the molecular analogue of (1.2). In the simplest case of a diatomic molecule

$$V_{n\ell\lambda}(R) = V^+(R) - \frac{R_y}{[n - \mu_{\ell\lambda}(R)]^2}, \tag{1.3}$$

Cambridge University Press
978-0-521-76995-2 - Theory of Molecular Rydberg States
M. S. Child
Excerpt
More information

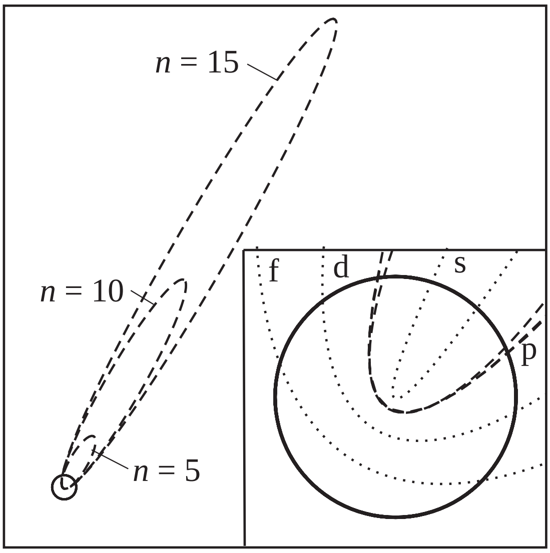

Figure 1.2 Semiclassical p orbits with $\ell = 1.5$ and $n = 5$, 10 and 15, compared with a core of radius $10a_0$. The inset shows that the two latter orbits are indistinguishable in the core region, with a small but discernible difference from the inner $n = 5$ orbit. The dotted curves in the inset follow the s, d and f orbits for $n = 10$.

where $V_{n\ell\lambda}(R)$ is the *ab-initio* potential function for $n = 3$ or 4 and $V^+(R)$ is the corresponding curve for the positive ion. An alternative, more powerful, *ab-initio* approach, particularly in the presence of potential surface crossings, is to solve the *ab-initio* equations within a relatively small box around the ionic core and to join the resulting Rydberg orbitals to combinations of the exact Coulomb functions in the outer region by what are called R-matrix methods [11, 12, 13].

The reader may wonder at this stage why it is legitimate to employ the output from *ab-initio* calculations, which are performed within the fixed nucleus ‘Born–Oppenheimer’ approximation, despite the stated aim in the second paragraph to handle situations in which the electronic energy separations are small even compared with rotational ones. The answer again lies in the fact that the relevant perturbations to the electronic motion occur at short range, where the electron velocity is high. Figure 1.2 shows the equivalent classical orbits of a hydrogenic p electron, with $n = 5$, 10 and 15. The total orbit times are roughly equal to n^3 times the atomic time unit, $\tau = 2.417 \times 10^{-17}$ s, but an application of classical angle-action theory[1] shows that the fractional time within a core of radius 10 atomic units decreases as n^{-3}. Hence the transit time, and even the shape of the track in the inset

---

[1] Appendix E.5 of Child [14] shows that

$$r = n^2 a_0 (1 + \varepsilon \cos u),$$

in Fig. 1.2, are almost independent of n. Finally, as discussed in the footnote, the transit time itself varies from 1.2×10^{-16} s for an s orbit to 1.6×10^{-16} s for an f orbit, which is short compared with any molecular vibrational or rotational period. The Born–Oppenheimer approximation is therefore fully justified over the period during which the electron is perturbed by the core.

This classical argument has two other significant consequences. In the first place the n^{-3} dependence of the transit time for any bound orbit translates into an $n^{-3/2}$ dependence of the wavefunction amplitude within the core, which gives rise to a variety of Rydberg scaling laws. Secondly, the abruptness of the transit allows the use of a powerful 'frame transformation' technique [6]. The uncoupled states $|i\rangle$ in the outer region apply to the combination of a positive ion in a well-defined quantum state and an independent incoming or outgoing electron with defined angular momentum ℓ. The interaction region on the other hand supports Born–Oppenheimer states, $|\alpha\rangle$, in which the electron occupies a molecule fixed orbital with fixed instantaneous bond lengths. Moreover, an electron starting from an asymptotic state $|i\rangle$ typically switches to a Born–Oppenheimer core state $|\alpha\rangle$, so rapidly that the transition amplitude may be approximated as the simple projection $\langle i\,|\alpha\rangle$. The influence of the positive ion core is then taken into account via the quantum defects, μ_α, which cause phase changes between the incoming and outgoing wavefunctions. As a result the scattering from incident state $|i\rangle$ to final asymptotic state $|\,j\rangle$ may be characterized by matrices of the exponential or trigonometric forms, with elements of the form

$$S_{ij} = \sum_\alpha \langle i\,|\alpha\rangle\, \mathrm{e}^{2\mathrm{i}\pi\mu_\alpha} \langle\alpha\,|\,j\rangle \quad \text{or} \quad K_{ij} = \sum_\alpha \langle i\,|\alpha\rangle \tan\pi\mu_\alpha \langle\alpha|\,j\rangle. \tag{1.4}$$

---

where ε is the eccentricity

$$\varepsilon = \frac{\sqrt{n^2 - (\ell + 1/2)^2}}{n}$$

and u is an auxiliary variable, in terms of which the classical angle α_n is given by

$$\alpha_n = u + \varepsilon \sin u.$$

It is readily verified that the closest approach at $r = a_{n\ell} = n^2 a_0(1 - \varepsilon)$, which is approximately independent of n for $n^2 \gg (\ell + 1/2)^2$, is reached at $u = \alpha_n = \pi$.

Since α_n is designed to vary linearly with time, the fractional time to cross a spherical core of radius r_c is given by $[\alpha_n(r_\mathrm{c}) - \pi]/\pi$. One may assume a quadratic expansion for $\cos u$ about $u = \pi$, which is valid for

$$(u - \pi)^2 = \frac{\Delta_\mathrm{c}}{n^2\varepsilon} \ll 1,$$

where Δ_c is the scaled displacement $2(r_\mathrm{c} - a_{n\ell})/a_0$. The corresponding cubic expansion for $\sin u$ rearranges to

$$\frac{\tau_\mathrm{core}}{\tau_\mathrm{orbit}} = \frac{\alpha_n(r_\mathrm{c}) - \pi}{\pi} = \frac{\sqrt{\Delta_\mathrm{c}}\,[3(\ell + 1/2)^2 + \Delta_\mathrm{c}]}{6\pi n^3},$$

which demonstrates the n^{-3} dependence. A computation based on following the evolution of α_n and r as functions of the auxiliary variable u readily shows that the fractional angle action range within a core of radius $10\,a_0$ varies between $4.9n^{-3}$ for an s orbit to $6.7n^{-3}$ for an f orbit, which translates into a range of transit times from 1.2×10^{-16} s to 1.6×10^{-16} s.

Cambridge University Press
978-0-521-76995-2 - Theory of Molecular Rydberg States
M. S. Child
Excerpt
More information

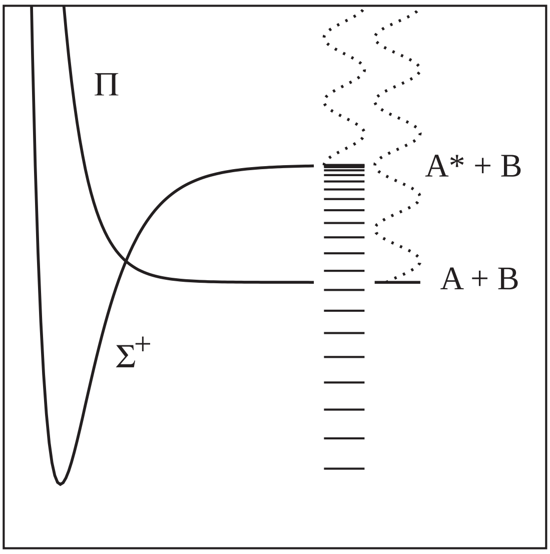

Figure 1.3 Schematic potential curves for a hypothetical AB molecule. Two continua are shown by wavy lines. One starts from the A + B asymptote of the repulsive Π curve. The other has an attached ladder of vibrational levels terminating on the $A^* + B$ dissociation limit of the bound Σ^+ curve.

We shall see in later chapters that the choice of an S- or a K-matrix depends on whether the scattering is formulated in terms of incoming and outgoing waves, or in terms of sine-like and cosine-like standing waves.

It is also helpful to introduce the concept of a ‘channel’, which plays an important role in any scattering formulation. Seen in a familiar framework, consider the potential curves of a hypothetical diatomic molecule in Fig. 1.3, each of which may be labelled by the electronic symmetry, by the states of its separated atom fragments, and by the total angular momentum. Each ‘channel’ then consists of the entire family of bound and continuum states, supported by the relevant potential curve, or ‘channel potential’. Since the diagram is actually drawn for $J = 0$, the bound levels of the Σ^+ potential belong to the rotationless vibrational states. The corresponding channel potentials for $J \neq 0$ include an additional centrifugal term, $J(J+1)\hbar^2/2\mu R^2$, and the bound levels are rotational–vibrational ones. As another useful terminology, a channel is said to be ‘open’ (to fragmentation) at energies above the dissociation limit, ‘closed’ at energies between $V_{\min}$ and the dissociation limit, and ‘strongly closed’ or ‘forbidden’ for $E < V_{\min}$. Thus the Σ^+ channel is closed and the Π channel strongly closed below the A + B asymptote, while the Π channel opens at energies above this dissociation limit. Finally both channels are open above the $A^* + B$ dissociation limit. One also speaks of the bound levels of the Σ^+ channel ‘lying in the Π continuum’ at energies between the A + B and

Cambridge University Press
978-0-521-76995-2 - Theory of Molecular Rydberg States
M. S. Child
Excerpt
More information

$A^* + B$ limits. Symmetry forbids any interaction between the two $J = 0$ channels, but added angular momentum can lead to 'heterogeneous predissociation' with a selection rule $\Delta J = \pm 1$, induced by Coriolis coupling [15].

The channels in Fig. 1.3 are termed molecular dissociation channels, labelled by different electronic states of the fragment atoms. In the Rydberg context, the ionization channels are equally important. The relevant channel potentials are then centrifugally corrected Coulomb potentials, each supporting infinite series of electronic states; and the asymptotes belong to different electronic, vibrational and rotational energies of the positive ion. Figure 1.1 illustrates electronic energy ladders (or Rydberg series) terminating on the $|v^+, N^+\rangle = |0, 0\rangle$, $|0, 2\rangle$, $|0, 4\rangle$ and $|1, 0\rangle$ states of H_2^+. There are in fact many such ladders with different angular momenta. One of the first molecular applications of multichannel quantum defect theory [6] demonstrated the important connection between spectral perturbations below the $|0, 0\rangle$ limit and auto-ionization in the interval between the $|0, 0\rangle$ and $|0, 2\rangle$ limits, arising from rotationally induced interactions between the np series that are designated as $n\mathrm{p}\sigma\ {}^1\Sigma_u^+$ and $n\mathrm{p}\pi\ {}^1\Pi_u$ at low energies, where the Born–Oppenheimer approximation applies; and as np0 and np2, according to the relevant value of N^+, at energies close to ionization. To see how the interaction arises, it is interesting to refer to the structure of the scattering matrices in (1.4). The labels $|i\rangle = |N^+\ell J\rangle$ designate the positive ion rotational state, the electronic angular momentum ℓ and the total angular momentum J,[2] while the Born–Oppenheimer labels are $|\alpha\rangle = |\ell\Lambda J\rangle$, where Λ is the electronic angular momentum that gives the σ or π character. It follows from (1.4) that the scattering matrices will contain no off-diagonal terms unless the quantum defects μ_α differ from one Born–Oppenheimer channel to another. In other words, by reference to (1.3) the energies of the $n\mathrm{p}\sigma\ {}^1\Sigma_u^+$ and $n\mathrm{p}\pi\ {}^1\Pi_u$ electronic states must differ. The beauty of the MQDT formulation is that the n dependence of such energy separations is determined by the almost energy-independent quantum defects, $\mu_{\mathrm{p}\sigma}$ and $\mu_{\mathrm{p}\pi}$.

1.2 Organization of the text

Four of the following chapters cover aspects of multichannel quantum defect theory, with an emphasis in the early chapters on connections with traditional spectroscopic theory. Two subsequent chapters focus on photo-excitation and photo-ionization in the context of modern n-photon experiments. The final chapter concerns the manipulation of Rydberg states. Readers should note that much of the technical detail is placed in the appendices. In particular, those unfamiliar with molecular terminology will find the notation explained in Appendix F. In addition details

---

[2] We ignore vibrational complications for simplicity.

Cambridge University Press
978-0-521-76995-2 - Theory of Molecular Rydberg States
M. S. Child
Excerpt
More information

of the construction of parity-adapted basis states for different angular momentum schemes are included in Appendix C.

The quantum defect picture

Chapter 2 outlines the essential elements of multichannel quantum defect theory (MQDT) [7, 8, 9]. It starts from the assumption that the scattering problem between the outer Rydberg electron and the positive ion core has been solved – by methods that will be outlined in later chapters. The relevant quantum defects, μ_α, and scattering K-matrices, that monitor the strength of the Rydberg–core interaction are assumed to be known. The chapter is therefore concerned with the behaviour of this outer electron, moving in a pure Coulomb field, and with how this behaviour is modified by the K-matrix parameters and the boundary conditions as $r \to \infty$.

The flexibility to handle arbitrary Rydberg systems, from atoms to polyatomic molecules is introduced by showing how the supposedly known K-matrix elements determine combinations of Coulomb basis functions in each channel, which are simply independent solutions of the radial Schrödinger equation, at the chosen energy and orbital angular momentum. An analysis of the boundary conditions as $r \to \infty$ leads to the characteristic structure of the MQDT working equations, which depend on matrices with dimensions equal to the number of interacting channels, which is orders of magnitude smaller than the number of basis states required for a conventional diagonalization. The nature of typical solutions is illustrated by demonstrating close similarities between the bound state structure immediately below the ionization limit and the auto-ionizing resonances immediately above. Connections with the matrix formulation of traditional spectroscopic theory are also discussed.

Ab-initio *methods*

Chapter 3 concerns the *ab-initio* determination of the quantum defects and scattering K-matrices, which may be derived as functions of the nuclear coordinates. A short introductory section uses the case of H_2 to show how analogues of (1.3) and (1.4) may be used to extract diagonal and off-diagonal quantum defects from families of possibly strongly interacting high level *ab-initio* surfaces. Factors affecting the bond length dependence of the quantum defect functions, $\mu_{\ell\Lambda}(R)$ are also discussed.

Subsequent sections concern the formulation and implementation of what are termed R-matrix techniques, which allow the direct determination of the nuclear-coordinate-dependent $K(\mathbf{Q})$ matrix at arbitrary energies up to and above the ionization limit [11, 12, 13]. The argument is that the outer parts of all Rydberg wavefunctions behave as known Coulomb functions, outside the range of the Rydberg–core interactions. Thus the *ab-initio* effort may be restricted to a finite volume. The resulting inner wavefunction is then joined to the outer one by appropriate log-derivative boundary conditions at the core boundary, at which a strongly energy-dependent matrix $\mathbf{R}(E)$ ensures continuity between the inner and outer wavefunctions in the form

$$\psi_E(a) = \mathbf{R}(E)\left[a\psi'_E(a) + b\psi_E(a)\right], \tag{1.5}$$

where the components of the column vector $\psi_E(a)$ are the amplitudes of the Rydberg wavefunction in different channels at the core radius $r = a$, while b is a parameter appropriate to the nature of the internal basis functions. Continuity of the log-derivative at the boundary normally leads to the very weakly energy-dependent K-matrix, because the energy dependence of the R-matrix is cancelled by the log-derivatives of the outer basis functions.

Two types of R-matrix theory are discussed, according to whether the inner *ab-initio* equations are solved for electronic eigenvalues in a suitable continuum basis, perhaps with fixed log-derivatives in the early Wigner–Eisbud approach [16], or for eigenvalues of the log-derivative, $b(E)$, at a fixed energy in the eigenchannel method [13]. The convergence properties of the two methods are discussed, including the introduction of so called Buttle corrections to compensate for incompleteness in the Wigner method [17]. Illustrative applications of the two methods are described.

The treatment of species with large ion core dipoles is tackled in the final section.

Frame transformations and channel interactions

The strength of the theory is greatly enhanced by the use of frame transformations (Chapter 4), which are justified on one hand by the brevity of the 'core transit time', and more explicitly by demonstrating the insensitivity of the radial wavefunction to energy changes comparable to those associated with vibrations and rotations of the ion core. Both these lines of argument justify the conclusion that the transition amplitude between coupled and uncoupled representations may be accurately approximated by the simple internal overlap $\langle i\,|\alpha\rangle$. Subsequent sections of the chapter deal with the machinery required to perform rotational, vibrational and vibronic frame transformations, each of which is illustrated by appropriate physical applications.

Rotational frame transformation theory is complicated by the variety of angular momentum coupling schemes from one molecule to another [5, 18]. The treatment in the main text is therefore limited to the simplest case, in which spin is ignored, leaving more complicated situations to be handled in Appendix C. Applications are chosen to show how MQDT theory handles the familiar topics of Λ-doubling and ℓ-uncoupling [2, 5, 19]. It is also shown how decreasing electronic energy spacings as the energy increases are reflected in 'stroboscopic' fringes in the spectrum as periods of the electronic motion tune through integer multiples of the fixed rotational period.

The third section covers vibrational channel interactions, for which the vibrational wavefunctions, $\langle R|v^+\rangle$, of the positive ion play the part of frame transformation elements between the fixed nucleus Born–Oppenheimer and the uncoupled positive ion states. The forms of the resulting K-matrix elements $\langle v^{+\prime}|\tan \pi\mu_{\ell\lambda}(r)|v^+\rangle$ are well displayed by the np series of H_2, in view of the strong nuclear coordinate dependence of the pσ quantum defect. Applications to the discrete level structure and vibrational auto-ionization are given.

The final section of Chapter 4 starts with a brief discussion of vibronic curve-crossing interactions. A longer account of Jahn–Teller induced coupling throughout a Rydberg series is then described. Particular emphasis is given to the scaling of the coupling strength according to changes in the principal quantum number. The mechanism of Jahn–Teller-induced auto-ionization is also discussed as a prelude to the theory of dissociative recombination in the following chapter.

Predissociation and dissociative recombination

Chapter 5 extends the theory to include both ionization and dissociation channels as illustrated by the processes

$$\mathrm{AB}^+ + e \rightleftarrows \mathrm{AB}^* \rightleftarrows \mathrm{A} + \mathrm{B}.$$

Thus the central species AB^*, which designates a Rydberg state, may auto-ionize to left to produce a positive ion and an electron, or predissociate to the right into neutral fragments. Alternatively a collision between the electron and positive ion may yield neutral fragments in a process known as 'dissociative recombination' [20]. The reverse possibility, whereby the neutrals collide to produce ions is 'collisional ionization'.

Two treatments of these composite processes are described. The first employs a perturbation model, which is particularly appropriate to curve-crossing situations. It rests on combining the vibrational and rotational channel interaction theory of the previous chapter with a 'generalized MQDT' treatment of the dissociation dynamics, details of which are given in Appendix E. The two strands are linked by the perturbative construction of a global K-matrix with both ionization and dissociation channels. The same formal construction allows the treatment of dissociative recombination at higher energies, although the theory is more easily expressed in terms of a composite S-matrix than the corresponding K-matrix. The factors responsible for the magnitude and energy dependence of the cross-section are illustrated by reference to the dissociative recombination of H_2^+ and NO^+.